

Electronic Supplementary Information (ESI) for:

Fast magnesianation kinetics in α -Ag₂S nanostructures enabled by *in-situ* generated silver matrix

Zhuang Chen^{‡,a}, Zhonghua Zhang^{‡,a}, Aobing Du^b, Yuduo Zhang^a, Mingyang Men^a, Guicun Li^{*,a}, and
Guanglei Cui^{*,b}

^aCollege of Materials Science and Engineering, Qingdao University of Science and Technology,
Qingdao 266042, China

^bQingdao Industrial Energy Storage Research Institute, Qingdao Institute of Bioenergy and
Bioprocess Technology, Chinese Academy of Sciences, Qingdao 266101, P. R. China

E-mail: guicunli@qust.edu.cn; cuiql@qibebt.ac.cn

[‡]Zhuang Chen, Zhonghua Zhang contributed equally.

This file includes following contents:

1. Experimental section
2. Figures (Fig. S1 to S13)
3. Tables (Tab. S1 and S2)

1. Experimental section

1.1 Materials preparation

0.1 g of AgNO_3 and 0.1 g of $\text{CS}(\text{NH}_2)_2$ were dissolved into 200 mL of deionized water in a flask under stirring for 10 min. The solution above was refluxed at 80 °C for 2 h. The gray product was washed with deionized water and ethanol for several times, and dried at 60 °C for 12 h to obtain the Ag_2S particles.

Graphene oxide (GO) powder was firstly prepared using a modified Hummers method. 200 mg of GO powder was dispersed in 200 mL of deionized water by vigorous ultrasonication for 1 h to obtain a homogeneous GO suspension. Subsequently, 0.1 g of AgNO_3 and 0.1 g of $\text{CS}(\text{NH}_2)_2$ were added into the above suspension under stirring for 10 min. The mixture was refluxed at 80 °C for 2 h. After that, 75 μL of hydrazine hydrate (85 wt.%) was dropped into the solution with vigorous stirring at 80 °C for another 5 h. The $\alpha\text{-Ag}_2\text{S}/\text{rGO}$ composites were obtained by drying at 60 °C for 12 h after washing with deionized water and ethanol for several times.

1.2 Materials characterization

X-ray diffraction (XRD) measurement was conducted on a Bruker D8 diffractometer using Cu Ka radiation. Field emission scanning electron microscope (SEM) images were collected with a Hitachi S-4800 equipment. Transmission electron microscope (TEM), high resolution TEM (HRTEM) images, and energy dispersive spectrometry (EDS) elemental mappings were recorded using a JEOLJEM-2010F microscope. X-ray photoelectron spectroscopy (XPS) measurements were performed by a Perkin-Elmer PHI 550 spectrometer. Raman spectra were conducted on a LabRam HR Evolution Raman spectrometer under the excitation length of 532 nm. Thermogravimetric (TG) curve was obtained in air atmosphere from 25 to 800 °C at a heating

rate of 10 °C min⁻¹.

1.3 Electrochemical measurements

The electrochemical properties of as-prepared materials were performed by using CR2032 coin-type cells which were assembled in an Ar-filled glove box. The cathodes were fabricated by mixing as-prepared materials (60 wt%), Super P (30 wt%) and PVDF (10 wt%) using NMP as solvent to form a homogeneous slurry, and then coated onto a stainless steel foil and dried at 80 °C for 12 h. The glass fiber and polished Mg foil were employed as the separator and the anode, respectively. The mass loading of active material is 0.3–0.5 mg cm⁻². The electrolytes were 0.5 M (PhMgCl)₂-AlCl₃/THF (APC) electrolyte and 0.5 M MgCl₂-AlCl₃/DME (MACC) electrolyte as previously reported. Galvanostatic charge-discharge measurements were conducted on a LAND CT2001A battery testing system between 0.4 V and 2.0 V (vs. Mg). Cyclic voltammetry (CV) is tested on a Biologic VMP-300 electrochemical workstation at a scan rate of 0.1 mV s⁻¹. Electrochemical impedance spectroscopy (EIS) were also performed on a Biologic VMP-300 electrochemical workstation. For high temperature test at 50 °C, the coin cells were placed in a electro-thermal incubator (303-0A, Shanghai Yetuo Instrumentation co., LTD) and stood for 1 h before measurements began.

The *in-situ* XRD measurement was performed using an in-situ cell equipment which was assembled in an Ar-filled glove box. The cathode was prepared by mixing the α-Ag₂S, Super P, and poly(tetrafluoroethylene) (PTFE) with a weight ratio of 6:3:1 using ethanol as solvent. Then, the mixture was rolled into slice and cut into dish with a diameter of 2.0 cm. The mass of active material is 1.75 mg cm⁻². The APC electrolyte, glass fiber and polished Mg foil were employed as the electrolyte, separator and anode, respectively. Galvanostatic discharge measurement was

conducted on a LAND CT2001A battery testing system at 20 mA g^{-1} . Each in-situ XRD pattern was recorded every 10 minutes.

The energy densities are calculated by using the following formula: $E=C \times V$, where E represents the energy density of the electrode, and C is the discharged specific capacity and V refers to the average voltage during the discharging process. The specific capacity is calculated based on the weight of the $\alpha\text{-Ag}_2\text{S}$ nanostructures.

2. Figures (Fig. S1 to S13)

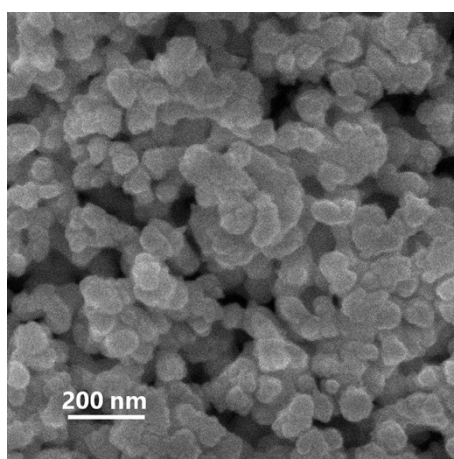


Fig. S1 The magnified SEM image of the $\alpha\text{-Ag}_2\text{S}$ nanostructures.

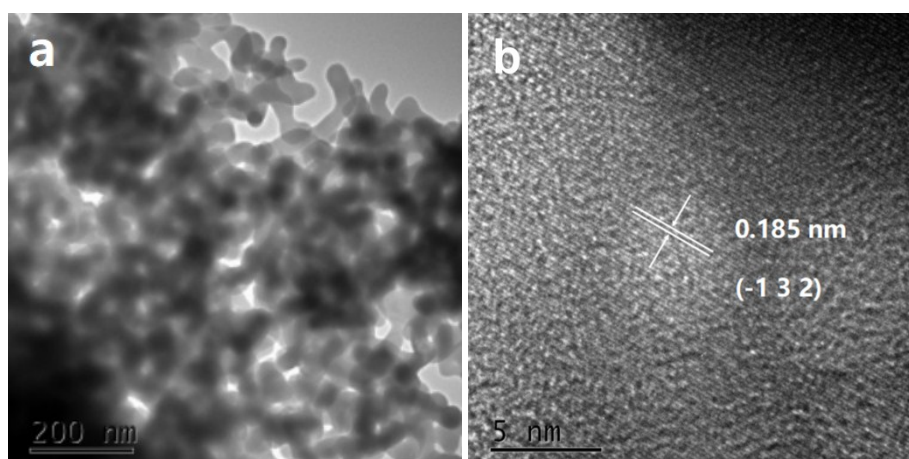


Fig. S2 The TEM image (a) and the HRTEM image (b) of the α -Ag₂S nanostructures.

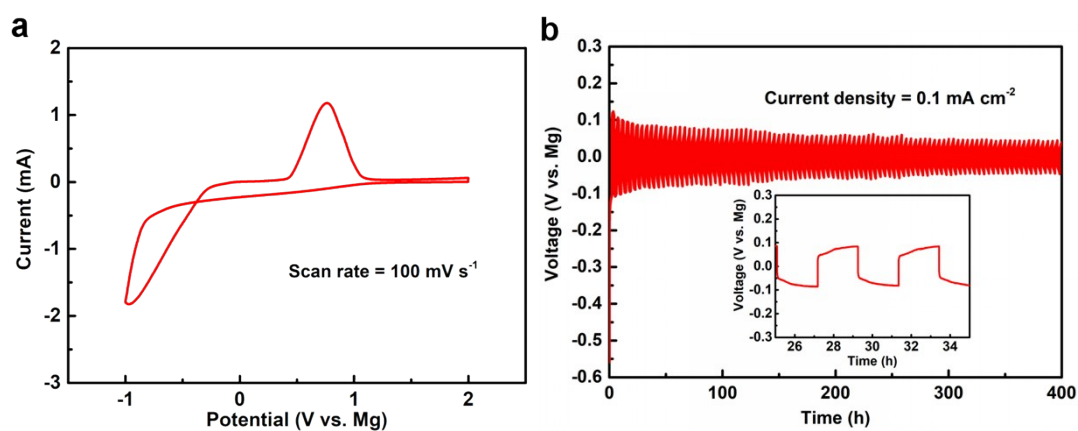


Fig. S3 The CV curve (a) of Mg||APC||SS cell at 100 mV s^{-1} in $-1.0 \sim 2.0 \text{ V}$; The cycling performance (b) of Mg||APC||Mg symmetrical cell at 0.1 mA cm^{-2} in 0.2 mAh cm^{-2} (inset shows magnified curves after several cycles).

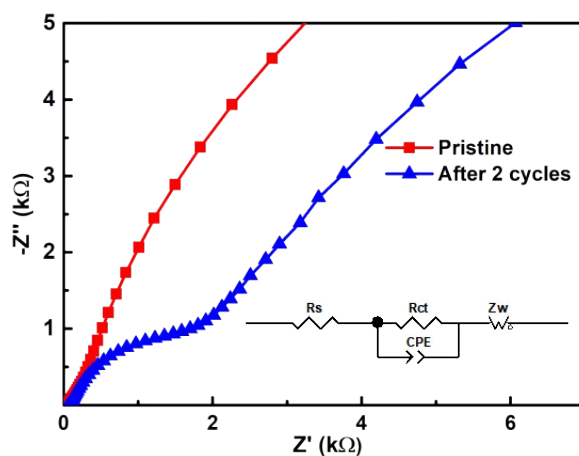


Fig. S4 The Nyquist plots of the α -Ag₂S cathode.

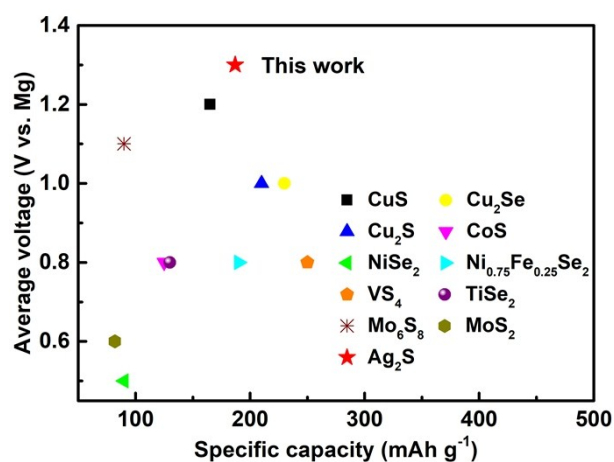


Fig. S5 Comparison of the α -Ag₂S nanostructures with other cathode of Mg batteries in terms of average voltage versus specific capacity.

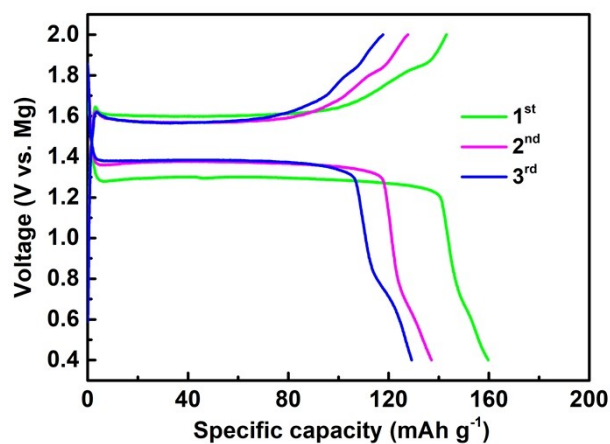


Fig. S6 The charge and discharge curves of the α -Ag₂S nanostructures with a mass loading of 1.5 mg cm⁻² at 10 mA g⁻¹.

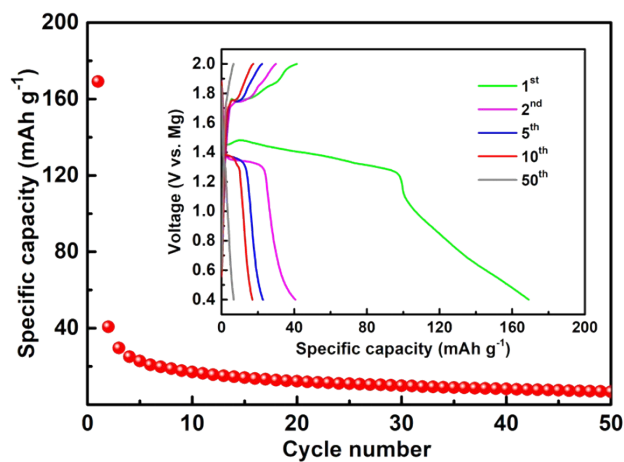


Fig. S7 The cycling performance of the α -Ag₂S nanostructures in MACC electrolyte at 50 mA g⁻¹ for 50 cycles. Inset shows the corresponding discharge-charge profiles.

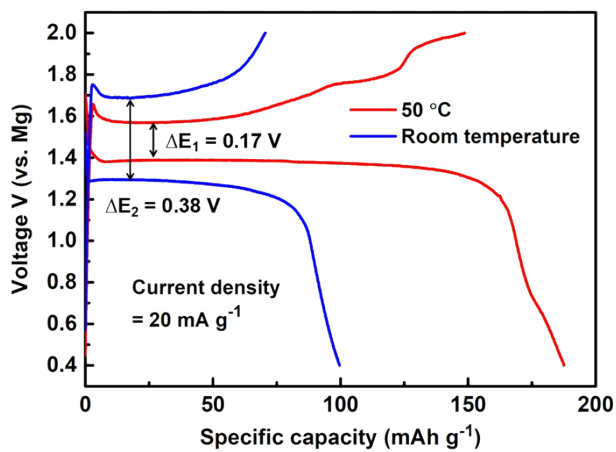


Fig. S8 The initial charge/discharge curves of the α -Ag₂S nanostructures at 20 mA g⁻¹ at different temperatures.

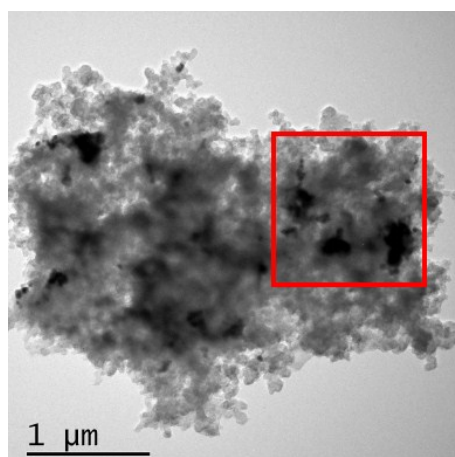


Fig. S9 The TEM image of the α -Ag₂S cathode after discharging to 0.4 V.

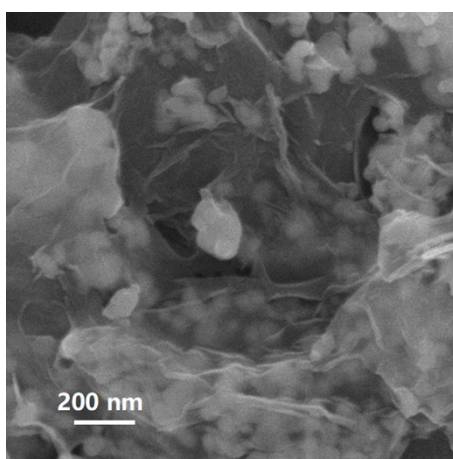


Fig. S10 The SEM image of the Ag₂S/rGO composite.

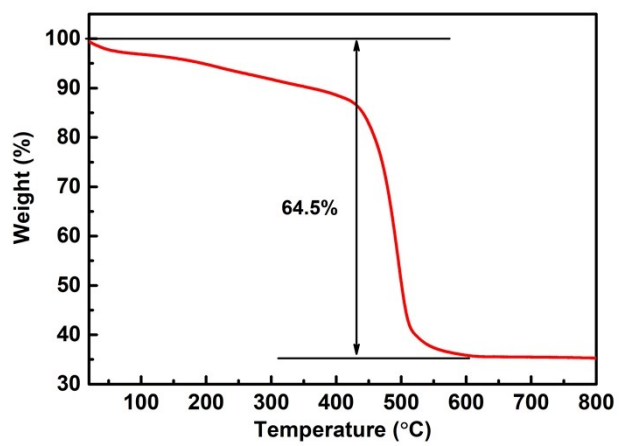


Fig. S11 The TG curve of the Ag₂S/rGO composite.

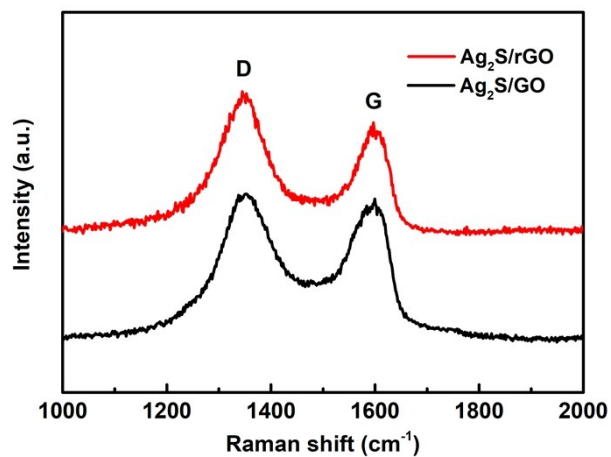


Fig. S12 Raman spectra of the α - $\text{Ag}_2\text{S}/\text{rGO}$ and α - $\text{Ag}_2\text{S}/\text{GO}$ samples.

Raman spectra of the α - $\text{Ag}_2\text{S}/\text{GO}$ and α - $\text{Ag}_2\text{S}/\text{rGO}$ samples show that the ratio of the D to G band intensity (I_D/I_G) increases from 1.02 to 1.15, indicating that GO is successfully converted to rGO by the low-temperature hydrothermal reduction.

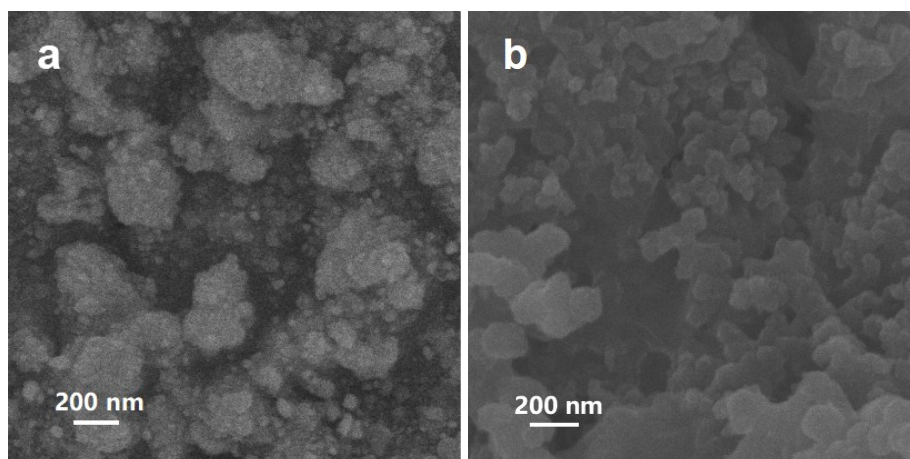


Fig. S13 The SEM images of the pristine Ag_2S electrode (a) and the $\text{Ag}_2\text{S}/\text{rGO}$ electrode (b) after long cycles at 1000 mA g^{-1} .

3. Tables (Tab. S1 and S2)

Tab. S1 Atomic parameters of the α -Ag₂S nanostructures.

Atom	#	OX	SITE	x	y	z	SOF	H	ITF(B)
Ag	1	+1	4e	0.758	0.015	0.305	1.	0	1.01
Ag	2	+1	4e	0.285	0.32	0.435	1.	0	1.16
S	1	-2	4e	0.359	0.239	0.134	1.	0	0.93

Tab.S2 Comparison of the electrochemical performance of other cathodes for various reported Mg batteries.

Cathode	Voltage (V vs. Mg)	Capacity (mA h g ⁻¹)	Gravimetric energy density (Wh Kg ⁻¹)	Density (Kg L ⁻¹)	Volumetric energy density (Wh Kg ⁻¹)	Loading (mg cm ⁻²)	Ref.
CuS	1.2	165	198	4.6	911	5.0-7.0	1
Cu ₂ S	1.0	230	230	6.6	1518	-	2
Cu ₂ Se	1.0	210	210	5.6	1176	-	3
CoS	0.8	125	100	5.9	590	-	4
NiSe ₂	0.5	90	45	6.8	306	1.77	5
Ni _{0.75} Fe _{0.25} Se ₂	0.8	190	152	6.8	1034	1.77	5
VS ₄	0.8	250	200	2.8	560	1.5-2.0	6
TiSe ₂	0.8	130	104	5.3	551	2.6-3.5	7
Mo ₆ S ₈	1.1	90	99	5.2	515	-	8
MoS ₂	0.6	82	49	5.1	251	1.0	9
α -Ag ₂ S	1.3	187	243	7.3	1762	0.3-0.5	This work
α -Ag ₂ S	1.3	160	208	7.3	1518	1.5	This work

Reference

1. F. Xiong, Y. Fan, S. Tan, L. Zhou, Y. Xu, C. Pei, Q. An and L. Mai, *Nano Energy*, 2018, **47**, 210-216.
2. M. Wu, Y. Zhang, T. Li, Z. Chen, S.-a. Cao and F. Xu, *Nanoscale*, 2018, **10**, 12526-12534.
3. Y. Tashiro, K. Taniguchi and H. Miyasaka, *Electrochim. Acta*, 2016, **210**, 655-661.
4. D. He, D. Wu, J. Gao, X. Wu, X. Zeng and W. Ding, *J. Power Sources*, 2015, **294**, 643-649.
5. L. Zhou, F. Xiong, S. Tan, Q. An, Z. Wang, W. Yang, Z. Tao, Y. Yao, J. Chen and L. Mai, *Nano Energy*, 2018, **54**, 360-366.
6. Y. R. Wang, Z. T. Liu, C. X. Wang, X. Yi, R. P. Chen, L. B. Ma, Y. Hu, G. Y. Zhu, T. Chen, Z. X. Tie, J.

- Ma, J. Liu and Z. Jin, *Adv. Mater.*, 2018, 30, 1802563.
7. Y. Gu, Y. Katsura, T. Yoshino, H. Takagi and K. Taniguchi, *Sci. Rep.*, 2015, **5**, 12486.
 8. D. Aurbach, Z. Lu, A. Schechter, Y. Gofer, H. Gizbar, R. Turgeman, Y. Cohen, M. Moshkovich and E. Levi, *Nature*, 2000, **407**, 724.
 9. Y. Liang, H. D. Yoo, Y. Li, J. Shuai, H. A. Calderon, F. C. Robles Hernandez, L. C. Grabow and Y. Yao, *Nano Lett.*, 2015, **15**, 2194-2202.